Redox Biology 30 (2020) 101425

Contents lists available at ScienceDirect

Redox Biology

journal homepage: www.elsevier.com/locate/redox

Transcription factor NRF2 uses the Hippo pathway effector TAZ to induce tumorigenesis in glioblastomas

Maribel Escoll[a,b,c,d], Diego Lastra[a,b,c,d], Marta Pajares[a,b,c,d], Natalia Robledinos-Antón[a,b,c,d], Ana I. Rojo[a,b,c,d], Raquel Fernández-Ginés[a,b,c,d], Marta Mendiola[e], Virginia Martínez-Marín[f], Isabel Esteban[f], Pilar López-Larrubia[a,b], Ricardo Gargini[g], Antonio Cuadrado[a,b,c,d,*]

[a] Instituto de Investigaciones Biomédicas "Alberto Sols" UAM-CSIC, Spain
[b] Instituto de Investigación Sanitaria La Paz (IdiPaz), Spain
[c] Department of Biochemistry, Faculty of Medicine, Autonomous University of Madrid, Madrid, Spain
[d] Centro de Investigación Biomédica en Red Sobre Enfermedades Neurodegenerativas (CIBERNED), ISCIII, Madrid, Spain
[e] Laboratory of Pathology and Translational Oncology, Instituto de Investigación Sanitaria La Paz (IdiPaz), Madrid, Spain
[f] Department of Pathology, Instituto de Investigación Sanitaria La Paz (IdiPaz), Madrid, Spain
[g] Centro de Biología Molecular "Severo Ochoa" UAM-CSIC, Autonomous University of Madrid, Madrid, Spain

ARTICLE INFO

Keywords:
Oxidative stress
Cancer stem cells
Chemotherapy
Glioblastoma

ABSTRACT

Transcription factor NRF2 orchestrates a cellular defense against oxidative stress and, so far, has been involved in tumor progression by providing a metabolic adaptation to tumorigenic demands and resistance to chemotherapeutics. In this study, we discover that NRF2 also propels tumorigenesis in gliomas and glioblastomas by inducing the expression of the transcriptional co-activator TAZ, a protein of the Hippo signaling pathway that promotes tumor growth. The expression of the genes encoding NRF2 (*NFE2L2*) and TAZ (*WWTR1*) showed a positive correlation in 721 gliomas from The Cancer Genome Atlas database. Moreover, NRF2 and TAZ protein levels also correlated in immunohistochemical tissue arrays of glioblastomas. Genetic knock-down of NRF2 decreased, while NRF2 overexpression or chemical activation with sulforaphane, increased TAZ transcript and protein levels. Mechanistically, we identified several NRF2-regulated functional enhancers in the regulatory region of *WWTR1*. The relevance of the new NRF2/TAZ axis in tumorigenesis was demonstrated in subcutaneous and intracranial grafts. Thus, intracranial inoculation of NRF2-depleted glioma stem cells did not develop tumors as determined by magnetic resonance imaging. Forced TAZ overexpression partly rescued both stem cell growth in neurospheres and tumorigenicity. Hence, NRF2 not only enables tumor cells to be competent to proliferate but it also propels tumorigenesis by activating the TAZ-mediated Hippo transcriptional program.

1. Introduction

Glioblastomas (GBs) are the most common primary malignant brain tumors and remain incurable, with a poor survival rate after diagnosis. They present somatic mutations in receptor tyrosine kinase pathways, p53 and retinoblastoma, that correlate with their anatomopathological classification [1]. However, other effectors are less known.

NRF2 (Nuclear factor (erythroid-derived 2)-like 2), encoded by the gene *NFE2L2*, is a basic region-leucine zipper transcription factor that forms heterodimers with small musculoaponeurotic fibrosarcoma proteins (MAFs) in the nucleus [2]. The heterodimer recognizes an enhancer sequence termed antioxidant response element (ARE) that is present in the regulatory regions of more than 200 genes (ARE-genes). ARE-genes encode a broad network of enzymes involved in phase I, II, and III biotransformation reactions, antioxidant mechanisms encompassing NADPH-, glutathione- and thioredoxin-mediated reactions, lipid and iron catabolism, autophagy gene expression, etc. Through this complex transcriptional network, NRF2 coordinates multifaceted responses to diverse forms of stress for the maintenance of a stable internal environment [3,4]. It is now accepted that these homeostatic functions provide a growth advantage to cancer cells in the hostile tumor microenvironment and promote cancer progression [5], metastasis [6], and resistance to chemo- and radiotherapy [7–9]. Its activity is generally increased in glioblastoma cell lines [10] and tumors [11], and elimination of NRF2 expression inhibits the proliferation and self-renewal of glioma stem cells [11].

* Corresponding author. Instituto de Investigaciones Biomédicas "Alberto Sols" UAM-CSIC, C/ Arturo Duperier, 4, 28029, Madrid, Spain.
E-mail address: antonio.cuadrado@uam.es (A. Cuadrado).

https://doi.org/10.1016/j.redox.2019.101425
Received 17 October 2019; Received in revised form 22 December 2019; Accepted 31 December 2019
Available online 02 January 2020

The tumor promoting activity of NRF2 has been attributed to its homeostatic functions. However, embryonic, pluripotent and cancer stem cells express high NRF2 levels [12–14] under controlled *in vitro* culture conditions, suggesting additional pro-tumorigenic functions. NRF2 controls the expression of the stemness associated protein Notch1 [15], while NRF2 inactivation affects stem cell renewal [13,14,16]. However, a mechanistic connection between stemness and NRF2 has not been demonstrated yet. Here, we focused on the Hippo pathway effector TAZ (Transcriptional co-activator with PDZ-binding motif). The Hippo pathway is a Ser/Thr phosphorylation-dependent cascade that, through the YAP and TAZ co-activators of TEADs1-4, participates in regulation of organ development, cell proliferation, migration, invasion, and stemness in multiple human cancers [17]. TAZ, encoded by the gene *WWTR1*, is a crucial element of the Hippo signaling pathway. Its expression is elevated in several tumor types including gliomas [18] and correlates with the grade of malignancy, being maximal in glioblastomas [19]. Patients with TAZ over-expressing tumors exhibit a poor prognosis, and, in cell models, TAZ promotes tumor progression, while its knockdown prevents proliferation, tumorigenicity and invasion of glioma cells [19]. TAZ is exquisitely regulated at the level of protein stability by a wide range of stress signals such as mechanical stress, low energy status, hypoxia and osmotic stress [20,21]. These signals activate the Hippo pathway, leading to TAZ phosphorylation and subsequent cytoplasmic retention and degradation [22,23]. However, little is known about the regulation of its encoding gene, *WWTR1*.

In this study we analyzed if NRF2 might activate the Hippo pathway at the level of TAZ, taking GBs as a model. We report that NRF2 induces the expression of *WWTR1*, which is partly required for its oncogenic activity. Thus, NRF2 delivers a growth, proliferative and survival signal through TAZ in glioblastomas, which is not directly related to redox metabolism or cytoprotection. These results provide a new strategy for targeted glioblastoma therapy at the level of NRF2 by reducing not only its cytoprotective function but also the TAZ-dependent growth and proliferative signature.

2. Materials and methods

2.1. Glioma database analyses

LGG and GB datasets were retrieved from The Cancer Genome Atlas (https://www.ncbi.nlm.nih.gov/pubmed/27157931) and analyzed for *NFL2L2* and *WWTR1* expression (https://xenabrowser.net/; https://www.ncbi.nlm.nih.gov/pubmed/24120142). Mutations in the Hippo pathway or other signaling genes were also analyzed from the TCGA datasets, which were downloaded respectively from cBioPortal (http://www.cbioportal.org/) and TCGA databases (http://tcga-data.nci.nhi.gov/docs/publications/lgggbm_2015), using the UCSC cancer browser.

2.2. Cell culture and reagents

The validated cell lines HEK293T, U-373 MG and U-87 MG were maintained in Dulbecco's Modified Eagle Medium supplemented with 10% fetal bovine serum. Human glioblastoma explants, GB1, GB2, GB3 and GB4, were kindly supplied by Dr Marta Izquierdo (Centro de Biología Molecular “Severo Ochoa” - Autonomous University of Madrid). Most experiments with these explants were performed with GB1 and GB3 because they exhibit the highest proliferative rates. All experiments were conducted under neurosphere culture conditions as described previously [24]. Inmortalized human neural stem cells derived from ventral mesencephalon of fetal brain (ReNcell) were plated onto Corning® Matrigel® hESC-Qualified Matrix (CORNING) and maintained in Neurobasal medium (Gibco) containing 2% B27 Supplement (Gibco) (v/v), 20 ng/ml recombinant human EGF (Peprotech), 20 ng/ml recombinant human basic FGF (Peprotech), 100 U/ml Penicillin/Streptomycin (Life Technologies) and 1% Amphotericin b solution (Lonza) in 5% CO_2 at 37 °C conditions. Sulforaphane (SFN) and GSH-MEE were purchased from Sigma-Aldrich. Limiting dilution assays were performed essentially as described in Ref. [25]. The final data and the statistical significances were calculated using the Extreme Limiting Dilution Analysis (ELDA) software (http://bioinf.wehi.edu.au/software/limdil/index.html) [25].

2.3. Immunoblotting

This protocol was performed as described in Ref. [26]. Briefly, cells were homogenized in lysis buffer (TRIS pH 7.6 50 mM, 400 mM NaCl, 1 mM EDTA, 1 mM EGTA and 1% SDS) and samples were heated at 95 °C for 15 min, sonicated and pre-cleared by centrifugation. Proteins were resolved in SDS-PAGE, transferred to Immobilon-P (Millipore) membranes and proteins of interest were detected with the following primary antibodies: NRF2 (homemade and validated in Ref. [27]), NQO1 (ab2346, Abcam), GAPDH (CB1001, Merck Millipore), YAP/TAZ (8418, Cell Signaling Techonology); pMST (49332, Cell Signaling Techonology); MST (14946, Cell Signaling Techonology); pLATS (8654, Cell Signaling Techonology); LATS (3477, Cell Signaling Techonology); LaminB (sc-6217, Santa Cruz Biotechnology). Proper peroxidase-conjugated secondary antibodies were used for detection by enhanced chemiluminescence (GE Healthcare).

2.4. Lentiviral and retroviral vector production and infection

Pseudotyped lentiviral vectors were produced in HEK293T cells transiently co-transfected with 10 μg of the corresponding lentiviral vector pWXL, 6 μg of the packaging plasmid pSPAX2 (12260, Addgene) and 6 μg of the VSV-G envelope protein plasmid pMD2G (12259, Addgene) using Lipofectamine Plus reagent according to the manufacturer's instructions (Invitrogen). Retrovirus supernatant was prepared by transfection of phoenix-Ampho cells (Garry Nolan, Baxter Laboratory in Genetic Pharmacology, Department of Microbiology and Immunology, Stanford University, 450 Serra Mall) with 5 μg of each plasmid using Lipofectamine Plus. Lentiviral vector shRNA control (shco) (1864, Addgene), several shNRF2-1 (NM_006164 TRCN0000273494), shNRF2-2 (NM_006164 TRCN0000007555) and shTAZ (NM_015472 TRCN0000370007) were purchased from Sigma-Aldrich (MISSION shRNA). The lentiviral vector pWPXL-NRF2-WT (NRF2) was homemade using as expression vector pWPXL (control) (12257, Addgene). The retroviral vectors used were: pBabePuro (1764, Addgene) and pBabePuroTAZ-WT (TAZ) (generous gift from Kun-Liang Guan). Cells were infected in the presence of 4 μg/ml polybrene (Sigma-Aldrich) and selected with 1 μg/ml puromycin (Sigma-Aldrich).

2.5. Chromatin immunoprecipitation (ChIP) assay

This protocol was performed as described in Ref. [26]. Briefly, cells derived from two different glioblastoma explants were grown under stemness conditions and allowed to form neurospheres. Neurospheres were trypsinized and fixed with 1% formaldehyde. For HEK293T, cells were transfected with plasmid pcDNA3-NRF2-$^{\Delta ETGE}$-V5 encoding a NRF2 cDNA that lacks the high-affinity binding site for KEAP1 and contains a V5 tag. DNA complexes were immunoprecipitated with either anti-NRF2 (homemade) and rabbit anti-IgG (ab37415, Abcam) for glioblastoma explants or anti-V5 (37–7500, Invitrogen) and mouse anti-IgG (ab18413, Abcam) antibodies for transfected HEK293T cells. qRT-PCR was performed with the primers shown in Supplementary Table S1. Samples from at least 3 independent ChIPs were analyzed.

2.6. Analysis of mRNA levels

Total RNA extraction and qRT-PCR were done as detailed in Ref. [28]. Primer sequences are shown in Supplementary Table S2. Data analysis was based on the ΔΔCT method, with normalization of the raw data to the housekeeping gene *GAPDH* (Applied Biosystems). All PCRs

were performed from triplicate samples.

2.7. Xenograft and intracranial tumorigenicity assays

Balb/c athymic Nude-Foxn1^{nu} mice (Harlan) were used for the xenograft (eight-week-old males) and intracranial (six-week-old females) tumor assays. U-373 MG or U-87 MG cells (10^6 cells in 0.1 ml PBS) were inoculated subcutaneously. For xenografts, tumor growth was examined every 5 days for up to 65 days. Tumor volume = $\pi/6 \times$ (mean diameter)^3 [29]. U-87 MG (10^5 cells in 2 μl PBS) or GB3 explant glioblastoma cells (2×10^5 cells in 2 μl PBS with 5 ng/μl recombinant human basic FGF and 5 ng/μl recombinant human EGF, both from Peprotech) were inoculated intracranially at the right hemisphere (1 mm anterior, 1.8 mm lateral to bregma and 3 mm intra-parenchymal). The Intracranial tumor assay protocol was performed as described previously [30].

2.8. Magnetic resonance imaging (MRI)

MRI experiments were performed on a Bruker AVANCE III system (Bruker Medical GmbH®) using a 7.0-T horizontal superconducting magnet, equipped with a gradient insert (60 mm inner diameter) with a maximum intensity of 360 mT/m and a 1H selective surface coil (23 mm diameter). For assessing the tumor growth, contrast enhanced T1-weighted (CE-T1W) imaging was acquired after the intraperitoneal administration of 0.3M-Gd-diethylenetriaminepentaacetic acid (Magnevist®) at a dose of 0.2 mmol/kg. Images were obtained with a spin-echo sequence and the following parameters: repetition time = 250 ms, echo time = 10 ms, averages = 6, acquisition matrix = 256 × 256, in-plane resolution of 78 × 78 μm^2, slice thickness = 1.0 mm and 10 slices in axial orientation (total acquisition time of 4.8 min). For assessing the edema, T2-weighted (T2W) spin-echo images were acquired with a rapid acquisition with relaxation enhancement sequence and the following parameters: repetition time = 2500 ms, echo time = 45 ms, averages = 5, RARE factor = 8, acquisition matrix = 256 × 256, in-plane resolution of 78 × 78 μm^2, slice thickness = 1.0 mm and 10 slices in axial orientation (total acquisition time of 5 min). During the procedure, the mice are anesthetized and their vital signs are controlled. Tumor volumes were measured from anatomical CE-T1W images with ImageJ software.

2.9. Immunohistochemistry

Four μm-thick sections of paraffin-embedded samples of glioblastoma tissue from patients treated at the Instituto de Investigación Sanitaria La Paz (IdiPaz, Madrid, Spain) were arrayed in a collection of three tissue microarray slides. Taken together, these slides encompassed 26 good tumor cores. Sections were deparaffinized and rehydrated in water, and antigen retrieval was carried out by incubation in 1 mM EDTA, 0.05% Tween 20, pH 8.0 at 50 °C for 45 min. Endogenous peroxidase and nonspecific antibody reactivity was blocked with peroxidase blocking reagent (Dako) at room temperature for 15 min. The sections were then incubated for 60–90 min at 4 °C with the corresponding peroxidase conjugated primary antibodies for NRF2 (PA1-38312, Thermo Fisher Scientific), TAZ (HPA007415, Sigma-Aldrich), NQO1 (ab34173, Abcam), ATRX (DIA-AX1, Dianova), IDH1 (DIA-H09, Dianova), ki67 (M7240, Dako) and developed with 3,3′-diaminobenzidine (DAB). Negative controls with goat serum replacing the primary antibody were used. The slides were mounted with DPX (VWR International). Detection was performed with the Envision Plus Detection System (Dako). All tumors were negative for IDH1 and ATRX mutations, therefore confirming that according to histological classification they were GBs. Densitometric quantification was done using macros of the ImageJ software.

2.10. Luciferase reporter generation and luciferase assay

Oligonucleotides with 3 tandem repetitions of the putative ARE2, ARE2-mutaded, ARE5, ARE6, ARE8 and ARE9 were cloned as detailed in Supplementary Table S3 and previously described [31]. Cells were transiently transfected with the expression vectors ARE2, ARE2-mutated, ARE5, ARE6, ARE8, ARE9 or positive control ARE-Luc. pTK-Renilla was also transfected as an internal control. Luciferase assays were performed with the Dual- Luciferase Reporter Assay System (Promega, E1910) as previously described [32].

2.11. Flow cytometry determination of reactive oxygen species

Intracellular reactive oxygen species (ROS) were detected in a FACScan flow cytometer (Becton-Dickinson) with hydroethidine (HE) (ThermoFisher Scientific), which upon oxidation emits orange fluorescence (BP 575/24 nm). Cells were incubated for 1 h at 37 °C with 2 μM HE and then detached from the plate, washed once with cold PBS, and analyzed immediately.

2.12. Statistical analyses

Data are presented as mean ± S.D. (standard deviation) or S.E.M. (standard error of the mean) as indicated in each case. Statistical assessments of differences between groups were analyzed using GraphPad Prism 5 software by the unpaired Student's t-test. For the scatter plots, the Pearson correlation coefficient (R) and the *p*-value associated with this coefficient were analyzed. Statistically significant differences in Kaplan-Meier survival curves were calculated with the log-rank test.

3. Results

3.1. Analysis of NFE2L2 and WWTR1 expression in glioblastomas (GBs)

We first analyzed the frequency of mutations in the genes *KEAP1*, and *NFE2L2*, encoding the main NRF2 repressor KEAP1 and NRF2, respectively, as well as several other growth-related pathways in 721 brain tumors from The Cancer Genome Atlas (TCGA) database. Only 11 tumors exhibited mutations in *KEAP1* or *NFE2L2* and only 32 in genes of the Hippo pathway (Fig. 1A). Low grade gliomas (LGGs) exhibited frequent mutations in *IDH1*, encoding Isocitrate Dehydrogenase-1 and *ATRX*, encoding ATP-dependent helicase. By contrast, GBs were prone to mutations in *EGFR*, encoding Epidermal Growth Factor Receptor, and *PTEN*, encoding Phosphatase and Tensin Homolog (Supplementary Fig. S1A). Additionally, we analyzed the mutation profile of gliomas with different levels *NFE2L2* and *WWTR1* expression (Fig. 1B). Low expression levels of *NFE2L2* and *WWTR1* were found in tumors with a high frequency of mutations in *IDH1* and *ATRX* while their high expression correlated with high frequency of mutations in *EGFR* and *PTEN*. It has been previously reported that LGGs exhibit low NRF2 levels, but the role of this factor in GB is poorly defined. In search for a mechanistic role of NRF2 in GBs, we focused in the Hippo pathway because the lack of frequent mutations might allow unmasking its physiological mechanism of regulation and its pathological subversion. We found a positive correlation in the levels of *NFE2L2* and *WWTR1* transcripts in both LGGs and GBs (Fig. 1C and D). Furthermore, we observed a striking similarity in the prognosis of *NFE2L2* and *WWTR1* overexpressing gliomas (Fig. 1E) and glioblastomas (Supplementary Figs. S1B and S1E). Additionally, we divided GBs as primary or secondary, according to their hypermethylation phenotype G-CIMP (glioma cytosine-phosphate-guanine (CpG) island methylator phenotype) which is associated with the *IDH* mutations characteristic of secondary glioblastomas [33,34] (Fig. 1E and Supplementary Figs. S1C, S1D, S1F and S1G). High expression of *NFE2L2* or *WWTR1* correlated with poor prognosis with an average of 1.7 years survival in gliomas (Fig. 1E) and 3 years in G-CIMP-positive glioblastomas (Supplementary

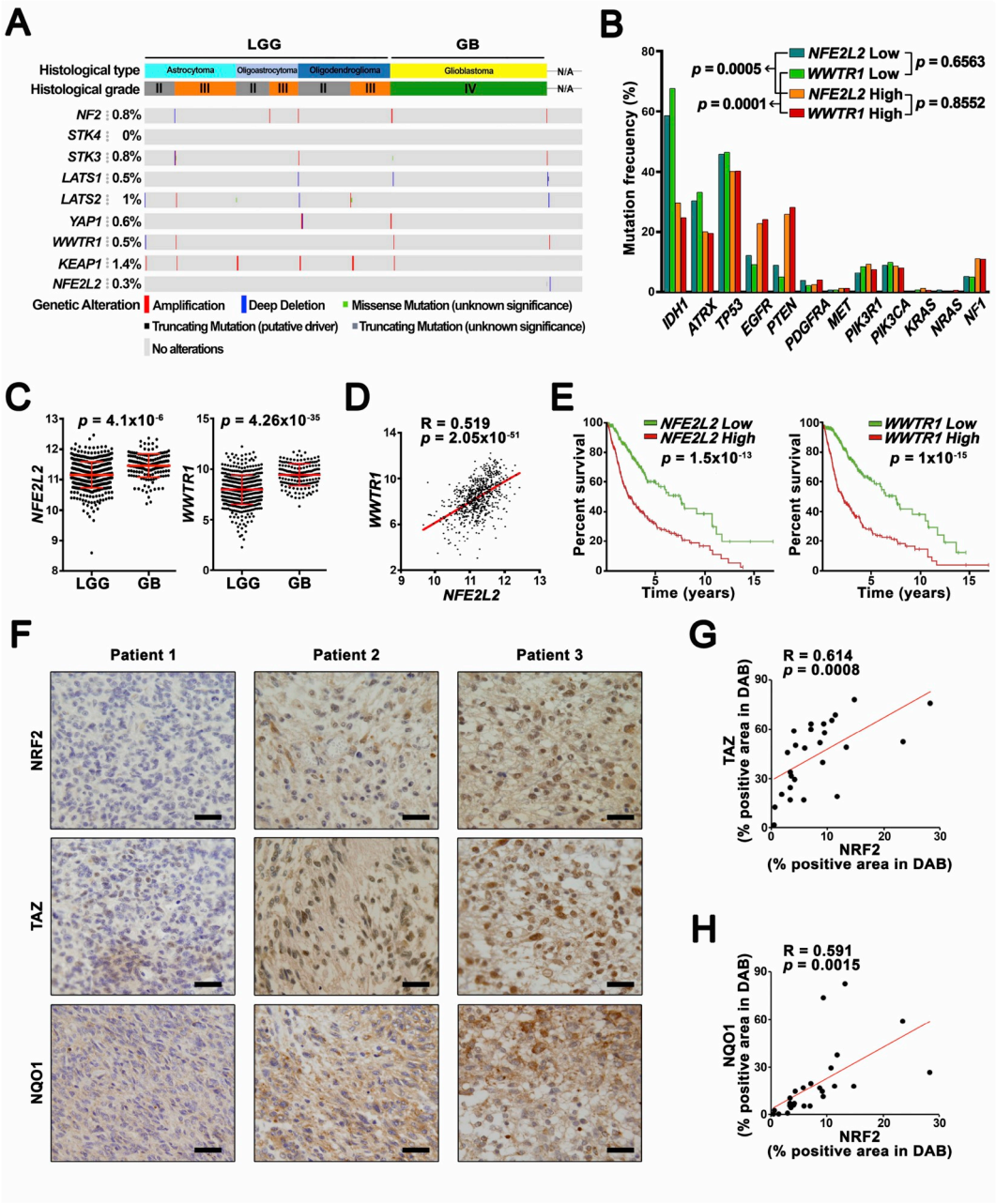

Fig. 1. Analysis of *NFE2L2* and *WWTR1* expression in GBs. **(A–E)** Analysis of *NFE2L2* and *WWTR1* expression in 721 gliomas from the TCGA database. **(A)** Analysis of somatic mutations in genes of the Hippo pathway, *KEAP1* and *NFE2L2*. **(B)** Analysis of the most frequent somatic mutations in gliomas (LGGs and GBs) grouped into high or low levels of *NFE2L2* compared to high or low levels of *WWTR1*. Statistical analysis was performed with Chi-square test for trend and *p*-value associated as indicated. **(C)** *NFE2L2* and *WWTR1* mRNAs are increased in GBs compared to LGGs. *p*-values for differences between groups are indicated in each graph and calculated using Student's t-test. **(D)** Scatter plot showing positive correlation between *NFE2L2* and *WWTR1* expression. The Pearson correlation coefficient (R) and the *p*-value associated with this coefficient are indicated. **(E)** Kaplan-Meier survival curves of patients with gliomas. Patients were stratified in two groups using *NFE2L2* or *WWTR1* Z-score values. Statistically significant differences in survival between groups were calculated using the log-rank test. **(F– H)** NRF2 and TAZ protein levels are positively correlated in GBs. A tissue array of 26 glioblastomas was analyzed. **(F)** Sections of three representative tumors with antibodies against NRF2, TAZ and NQO1 (scale bar, 50 μm). **(G, H)** Scatter plot showing positive correlation between densitometric quantification of DAB-staining (as percentage of area) of NRF2 and TAZ **(G)** or NRF2 and NQO1 **(H)**. The Pearson correlation coefficient (R) and the *p*-value associated with this coefficient are indicated. See also Supplementary Fig. S1.

Figs. S1D and S1G).

We further investigated NRF2 and TAZ protein levels in a tissue array of 26 histologically-defined GBs, all of which were negative for *IDH1* and *ATRX* mutations (Supplementary Fig. S1H). As an added control of NRF2 activity, we analyzed the downstream regulated gene product NADP(H) quinone oxidoreductase (NQO1). Fig. 1F shows three representative GBs with correlatively low, medium and high levels of NRF2, TAZ and NQO1 proteins. Densitometric quantification further demonstrated a statistically significant correlation in the expression of NRF2, TAZ and NQO1 proteins (Fig. 1G and H). Moreover, there was a positive correlation in the expression of NRF2 and TAZ with the proliferation marker ki67 (Supplementary Figs. S1I and S1J). Considering the strong correlation observed in prognosis, transcript and protein levels, in the following experiments we studied a potential mechanistic connection between NRF2 and TAZ.

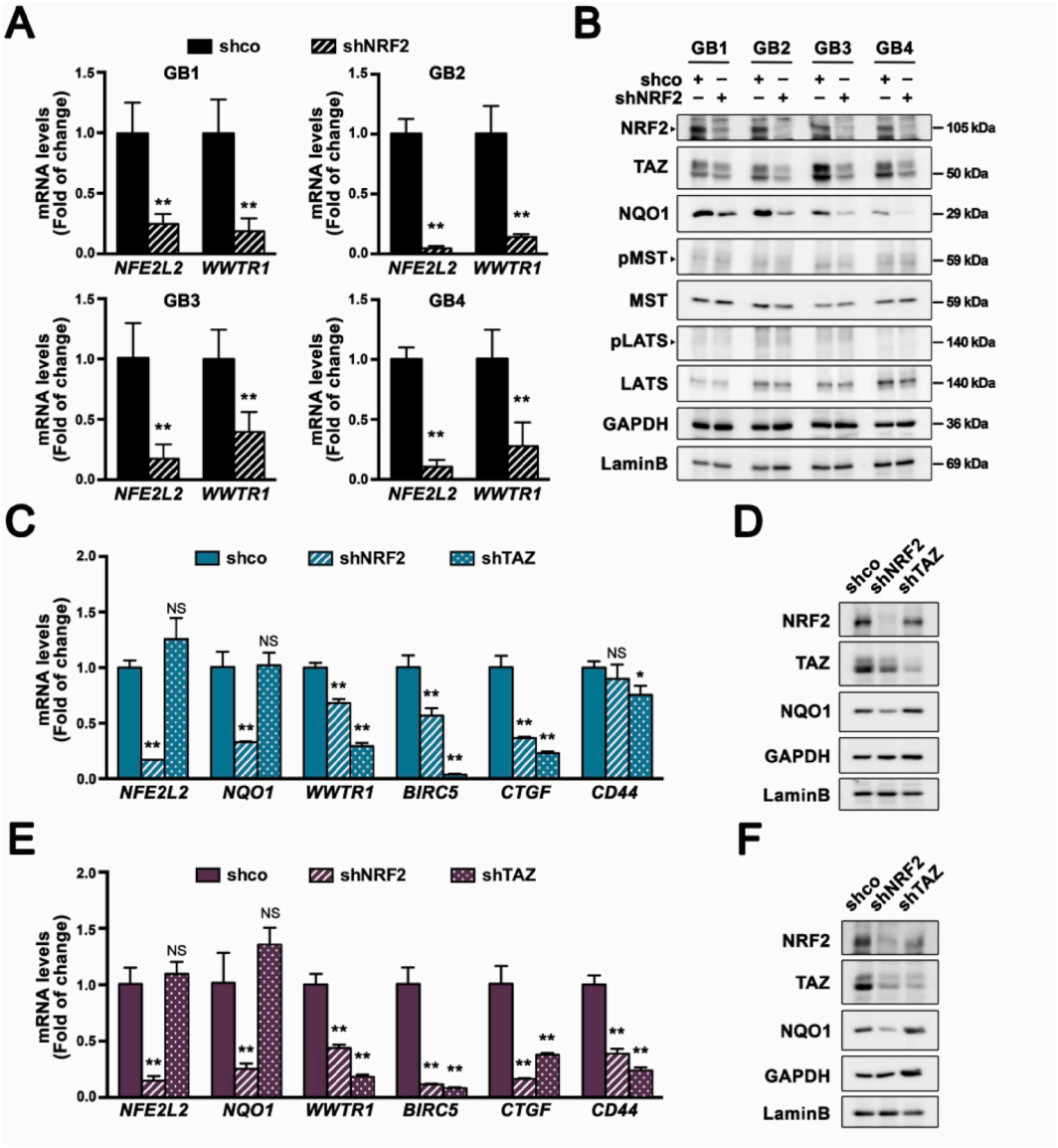

Fig. 2. NRF2 knocked-down cells exhibit decreased TAZ levels. **(A, B)** Four human glioblastoma explants (GB1, GB2, GB3 and GB4) were transduced with a lentivirus encoding control shRNA (shco) or human shNRF2. **(A)** mRNA levels of *NFE2L2* and *WWTR1* were determined by qRT-PCR and normalized by *GAPDH*. Data are mean ± S.D. (n = 3). Statistical analysis was performed with the Student's t-test. $^{**}p \leq 0.01$. **(B)** Representative immunoblots of NRF2, TAZ, NQO1, p-MST, MST, pLATS, LATS and GAPDH and LaminB as loading controls (n = 3). **(C, D)**, U-373 MG and **(E, F)** U-87 MG glioblastomas cell lines were transduced with lentiviral vectors containing shcontrol (shco), human shNRF2 or human shTAZ. **(C, E)** mRNA levels of *NFE2L2, NQO1, WWTR1, BIRC5, CTGF* and *CD44* were determined by qRT-PCR and normalized by *GAPDH*. Data are mean ± S.D. (n = 3). Statistical analysis was performed with the Student's t-test. $^{**}p \leq 0.01$; (NS, indicated not statistically significant). **(D, F)** Representative immunoblot analysis of NRF2, TAZ, NQO1 and GAPDH and LaminB as loading controls (n = 4). Similar results were obtained with a different shNRF2 (Supplementary Fig. S2).

3.2. Changes in NRF2 expression modify TAZ levels in tumor explants and cell lines

Four explants originated from independent GBs were lentivirally-transduced for 7 days with short hairpin RNAs, control (shco) or specific for NRF2 knock-down (shNRF2) (Fig. 2A and B). Efficient knock-down of NRF2 was confirmed at both the mRNA and protein levels to just 10–20% of its original expression levels. As expected, NRF2 knock-down led to the down-regulation of the *bona fide* NRF2 target NQO1 but, importantly, also led to a decrease of TAZ transcript and protein levels without changes in the phosphorylation status of upstream regulators of the Hippo pathway, MST and LATS.

We further extended these observations to the GB cell lines U-373 MG and U-87 MG. In agreement with the results obtained in the tumor explants, lentiviral knock-down of NRF2 for 7 days in U-373 MG cells led to a reduction of *NQO1*, as a control, as well as *WWTR1* and two of its targets *BIRC5* and *CTGF* (with subtle changes in *CD44*) (Fig. 2C and D). By contrast, TAZ knock-down reduced the expression of *WWTR1* and its targets but did not have a significant effect on the mRNA levels of *NFE2L2* or *NQO1*. Similar results were found in U-87 MG cells (Fig. 2E and F). Besides, NRF2 knock-down did not modify the phosphorylation status of the Hippo regulators MST and LATS (Supplementary Fig. S2A). Moreover, a time-course of lentiviral knock-down of NRF2 further demonstrated a progressive reduction in transcript and protein levels of NQO1 as expected but also of TAZ (Supplementary Figs. S2B and S2C). As added controls, another shNRF2 lentivirus yielded comparable results (Supplementary Figs. S2D and S2E) and ectopic expression of NRF2 in the shNRF2-knocked-down cells rescued *WWTR1* levels (Supplementary Fig. S2F). These results show that NRF2 is required for expression of TAZ.

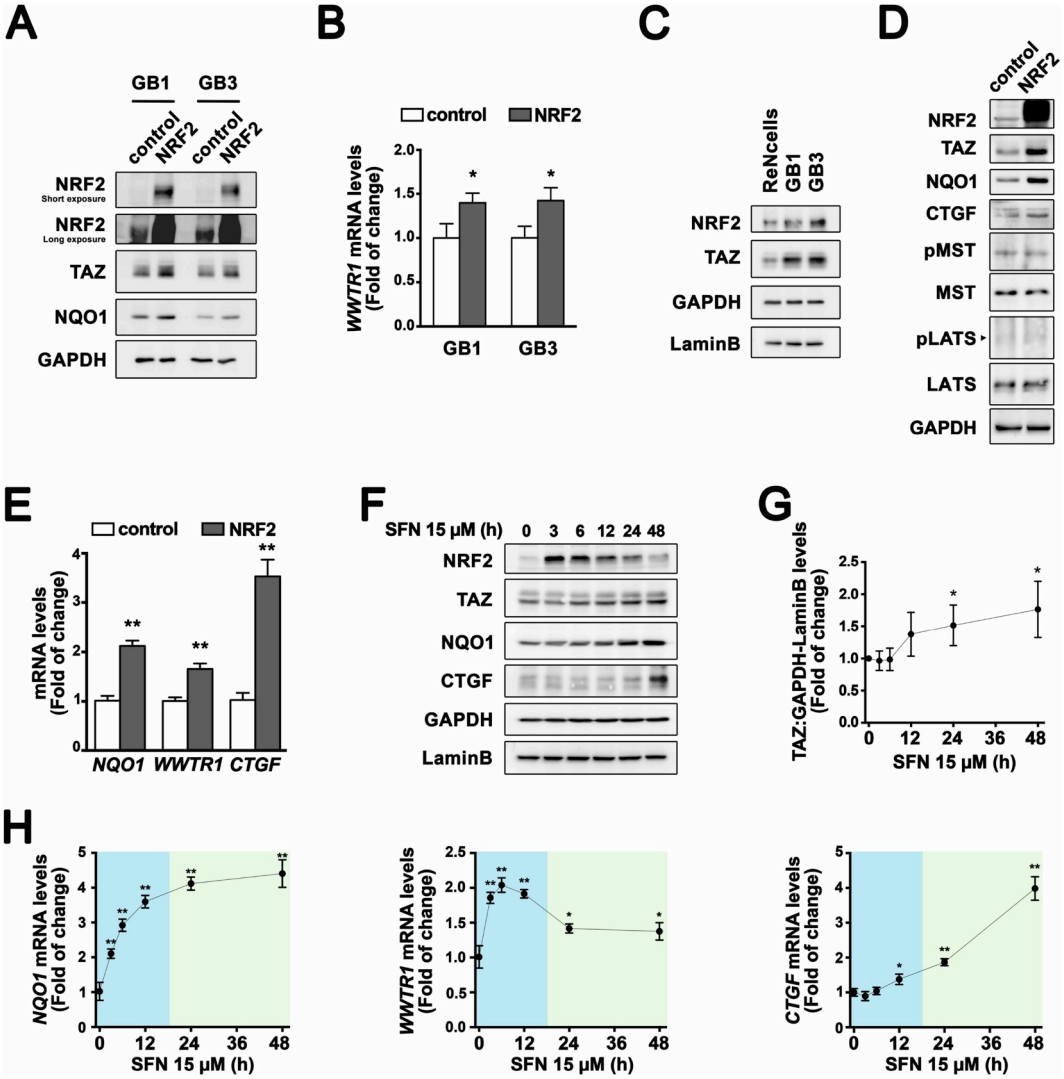

Fig. 3. Genetic and pharmacological up-regulation of NRF2 increases TAZ levels. **(A, B)** GB1 and GB3 glioblastoma cells were transduced with empty vector or lentiviral vector for overexpression of NRF2. **(A)** Representative immunoblot analysis of NRF2, TAZ, NQO1 and GAPDH as a loading control (n = 3). **(B)** Messenger RNA (mRNA) levels of *WWTR1* were determined by qRT-PCR and normalized by *GAPDH*. Data are presented as mean ± S.D. (n = 3) $^{**}p \leq 0.01$ according to a Student's t-test. **(C)** Representative immunoblots of NRF2, TAZ, GAPDH and LaminB as loading controls in ReNcell, GB1 and GB3. **(D, E)** ReNcell were transduced with empty vector or lentiviral vector for overexpression of NRF2. **(D)** Representative immunoblots of NRF2, TAZ, NQO1, CTGF, p-MST, MST, pLATS, LATS and GAPDH as a loading control (n = 3). **(E)** Messenger RNA (mRNA) levels of *NQO1*, *WWTR1* and *CTGF* were determined by qRT-PCR and normalized by *GAPDH*. Data are presented as mean ± S.D. (n = 3) $^{**}p \leq 0.01$ according to a Student's t-test. **(F– H)** ReNcell cells were treated with sulforaphane (SFN) (15 μM) for the indicated times. **(F)** Representative immunoblots of NRF2, TAZ, NQO1, CTGF, GAPDH and LaminB as loading controls (n = 3). **(G)** Densitometric quantification of TAZ levels representative blots from **(F)** relative to GAPDH and LaminB levels. Data are mean ± S.D. (n = 3) $^{*}p \leq 0.05$ according to a Student's t-test. **(H)** Messenger RNA (mRNA) levels of *NQO1*, *WWTR1* and *CTGF* were determined by qRT-PCR and normalized by *GAPDH*. Data are presented as mean ± S.D. (n = 3) $^{**}p \leq 0.01$ according to a Student's t-test. The blue area represents the wave of NRF2 dependent transcription and the green area depicts a second wave that involves NRF2 and also TAZ-dependent transcription. The time for transition from one wave to the other is was chosen as a possible suggestion. See also Supplementary Fig. S3. (For interpretation of the references to colour in this figure legend, the reader is referred to the Web version of this article.)

Then, we used genetic and chemical strategies to upregulate NRF2. Lentiviral over-expression of NRF2 for 4 days led to a modest increase in TAZ and NQO1 mRNA and protein levels in two primary glioblastomas (GB1 and GB3) (Fig. 3A and B) and U-373 MG and U-87 MG cells (Supplementary Figs. S3A and S3B). The low effect of NRF2 overexpression might be due to the fact that glioma stem cells exhibit basally high NRF2 levels [35]. Moreover, under similar proliferation conditions the levels of NRF2 protein and *WWTR1* transcript are similar in the glioblastomas analyzed (Supplementary Figs. S3C and S3D). Therefore, we analyzed the effect of NRF2 overexpression in the non-tumorigenic ReNcell stem cell line, which exhibits low NRF2 expression (Fig. 3C **and** Supplementary Fig. S3E). Ectopic expression of NRF2 in these cells led to increased levels of control NQO1 protein and mRNA but also TAZ and its target CTGF without changes in upstream regulators MST and LATS of the Hippo pathway (Fig. 3D and E).

In order to analyze the temporal changes in the NRF2 and TAZ transcriptional signatures, we treated these cells with the NRF2 activator sulforaphane (SFN, 15 μM). NRF2 was stabilized within the first 3 h of treatment and then slowly decreased to basal levels at 48 h (Fig. 3F). This change correlated with a gradual accumulation of NQO1 and TAZ, first at the transcriptional level and then at the protein level (Fig. 3F, G and 3H). Although *WWTR1* gene induction was more modest than that for *NQO1,* at the protein level TAZ also remained significantly elevated for at least 48 h (Fig. 3G). Thereafter, *CTGF* transcript levels augmented slowly in a fashion consistent with the TAZ increase, further leading to the accumulation of CTGF protein by 48 h (Fig. 3F and H).

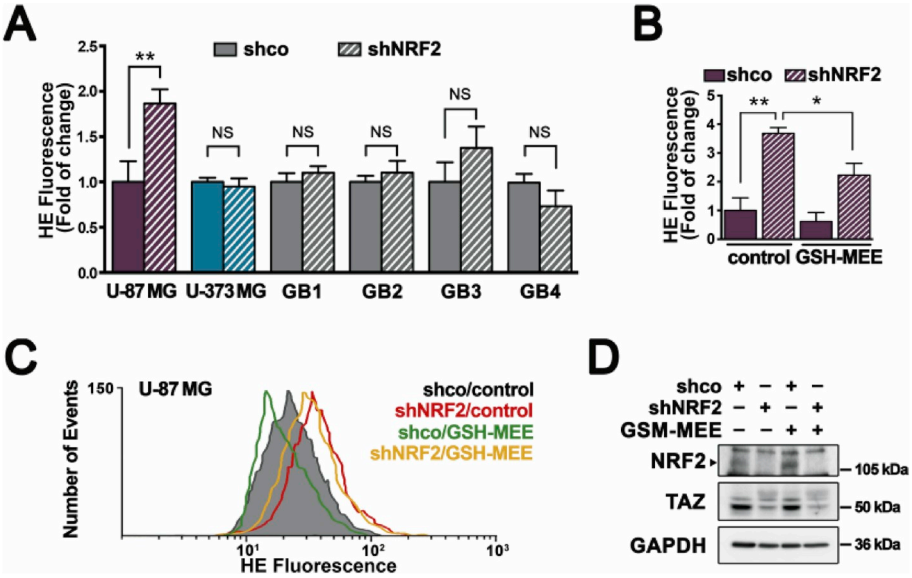

Fig. 4. The regulation of *WWTR1* by NRF2 is not dependent of the redox state. **(A)** U-87 MG and U-373 MG glioblastoma cells and four human glioblastoma explants (GB1, GB2, GB3 and GB4) were transduced with lentiviral vectors containing shcontrol (shco) or human shNRF2 and changes in intracellular ROS were determined by HE staining (n = 3). **(B–D)** U-87 MG glioblastoma cells were transduced with lentiviral vectors containing shco or human shNRF2 and treated with GSH-MEE (10 mM, 16 h). **(B, C)** Flow cytometry analysis of shNRF2-induced intracellular ROS production in HE stained cells. A representative sample of 10,000 cells is shown for each condition. **(D)** Representative immunoblots of NRF2, TAZ and GAPDH as a loading control (n = 3).

These results suggest a mechanistic connection between NRF2 and the TAZ transcriptional programme. Thus, a first wave of NRF2-dependent transcriptional activation that included NQO1 and TAZ (blue area in Fig. 3H) was followed by a second more modest wave where TAZ levels were high enough to increase the expression of the *CTGF* gene (green area in Fig. 3H).

3.3. The regulation of WWTR1 by NRF2 is not dependent of the redox state

NRF2 reinforces the antioxidant defense to tolerate the redox alterations of tumor cells. Therefore, we determined if the reduction of *WWTR1* expression in NRF2-depleted cells could be attributed to a modification of the redox environment. We silenced NRF2 in the four GB explants and the two GB cell lines, and measured the levels of reactive oxygen species (ROS) with the fluorescent probe hydroethidine (HE) by flow cytometry. As shown in Fig. 4A, NRF2-depletion did not increase ROS levels in any of the cell lines analyzed except U-87 MG, and yet there was a drastic reduction of TAZ protein levels, suggesting that the regulation of *WWTR1* by NRF2 is redox-independent. We further analyzed NRF2 knocked-down U-87 MG cells after incubation with the membrane permeable glutathione analog monoethylglutathione (GSH-MEE). The combination of NRF2 silencing and GSH-MEE exposure led to graded levels of HE fluorescence (Fig. 4B and C), and again TAZ levels were only dependent on NRF2 expression (Fig. 4D). These results indicate that NRF2 regulates TAZ by a redox-independent mechanism.

3.4. The WWTR1 promoter has functional NRF2-binding sites

We then looked for putative NRF2-regulated AREs in the *WWTR1* gene by using the Encyclopedia of DNA Elements at UCSC (ENCODE) (http://www.webcitation.org/query?url=https%3A%2F%2Fgenome.ucsc.edu%2F&date=2015-07-29) of the human genome (Feb. 2009). This database contains experimental data from chromatin immunoprecipitation (ChIP) studies of several transcription factors. Although NRF2 is not included, we analyzed three other ARE-binding factors, MAFK, MAFF and BACH1, for which information is available, and retrieved 9 putative ARE candidates according to the consensus sequence for NRF2 binding depicted at the JASPAR database (http://jaspar.genereg.net/) (Supplementary Table S4A). As shown in Fig. 5A, some of these AREs locate at transcriptionally active chromatin sites, as determined by the presence of DNAse and acetylation sensitive regions. Additionally, a similar analysis of the YAP coding gene (*YAP1*) showed three putative AREs with high score (Supplementary Table S4A and Supplementary Fig. S4A) and in fact, YAP was also down-regulated in NRF2-silenced GBs (Supplementary Figs. S3B and S3C). Focusing our study on TAZ, the nine putative AREs of the *WWTR1* gene were further analyzed by ChIP assays for endogenous NRF2 in two glioblastoma explants (Fig. 5B and Supplemental Table 4B). To avoid potential unspecific binding, we further confirmed these results with the immunoprecipitation of a V5 tagged-NRF2 construct in HEK293T transfected cells (Supplemental Fig. S5A) [36]. Immunoprecipitated DNA was analyzed by qRT-PCR with specific primers surrounding the putative AREs (Supplementary Table S1). At least 3 of the 9 putative AREs analyzed, termed ARE2, ARE5 and ARE6, exhibited high enrichment although not as strong as the positive controls *HMOX1* and *NQO1* (Fig. 5B and C and Supplementary Table S4B). No enrichment was detected with specific primers for *ACTB* or for an upstream region of *NQO1* that does not contain an ARE (*NQO1**) [26], carried as negative controls. We chose ARE2, ARE5, ARE6, ARE8 and ARE9 for additional characterization in reporter luciferase assays. Three tandem nucleotide sequences of these putative AREs were cloned in the promoter region of a luciferase reporter. As a negative control, we cloned ARE2 mutated in the most conserved T and G residues (Fig. 5D). Because GBs were difficult to transfect, we used U-87 MG. We found that NRF2 interference reduced the luciferase expression of ARE2, ARE5, ARE6 and ARE8 reporters while the ARE9 and the ARE2-mutated reporter did not respond at all (Fig. 5E). Additionally, HEK293T cells transiently co-transfected with these reporters plus increasing amounts of NRF2-$^{\Delta ETGE}$-V5 exhibited increased luciferase activity of ARE2 but not ARE2-mutated (Supplementary Fig. S5B). Altogether, these results indicate that NRF2 binds and activates several ARE sequences with probably different potency in the *WWTR1* gene promoter.

3.5. TAZ rescues neurosphere growth of NRF2 knocked-down glioma stem cells

Two different glioblastoma explants, GB1 and GB3, and both U-373 MG and U-87 MG cell lines were grown as glioma stem cells in the proper medium as floating spherical colonies, termed neurospheres [24,30,37]. These neurospheres correspond to glioma stem cells and it is now accepted that they are responsible for anticancer drug resistance and tumor relapse. Therefore, we tested the effect of depleting either NRF2 or TAZ under neurosphere growth conditions. Lentiviral knockdown of NRF2 or TAZ yielded GB1 (Fig. 6A- 6C), GB3 (Fig. 6D- 6F), U-87 MG cells and U-373 MG cells (data not shown) unable to grow as

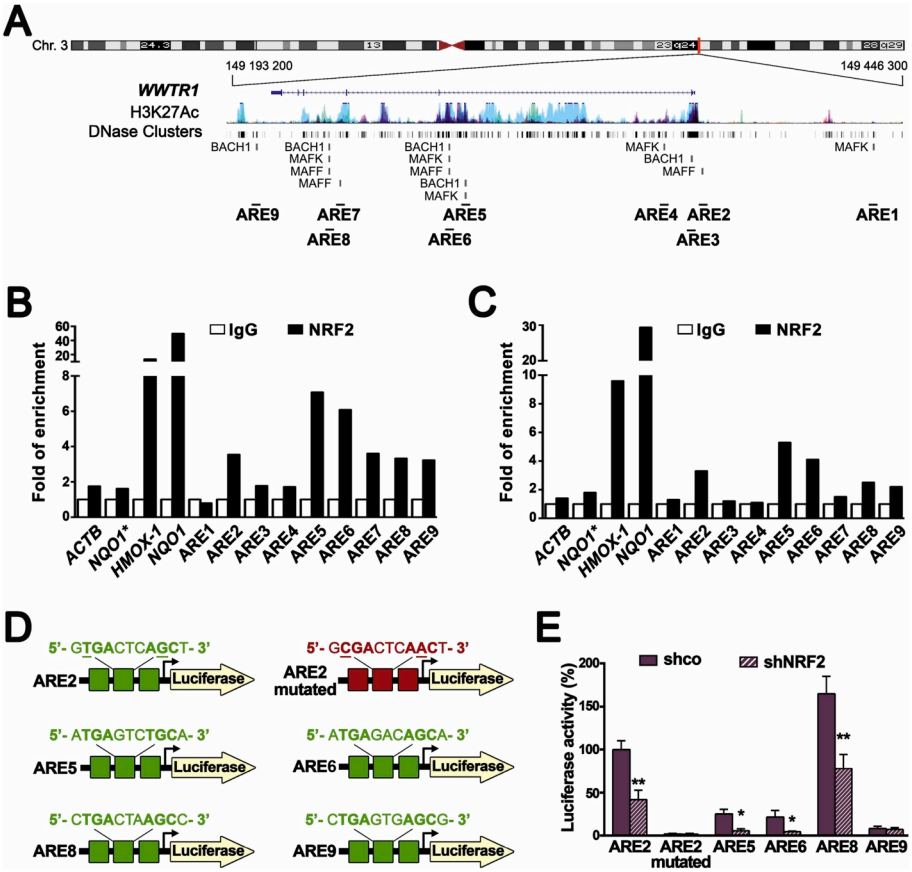

Fig. 5. The *WWTR1* promoter has functional NRF2-binding sites. **(A)** Representative scheme of the gene *WWTR1* encoding TAZ. Regions enriched in acetylated histone H3 lysine 27 (H3K27ac) are shown in blue and regions sensitive to DNase are represented as dark boxes. Experimental sequences reported to bind MAFK, MAFF and BACH1 factors were analyzed for the presence of AREs (ARE 1–9). **(B, C)** ChIP analysis of putative AREs found in **(A)** using the anti-NRF2 antibody vs. a control IgG in glioblastoma explant cells GB1 **(B)** and GB3 **(C)**. **(D)** Luciferase reporter constructs used for assessment of ARE2, ARE2 mutated, ARE5, ARE6, ARE8 or ARE9 functionality in pGL3basic vector. **(E)** U-87 MG glioblastomas cell lines were transduced with lentiviral vectors containing shco and human shNRF2 and transfected with ARE2, ARE2 mutated, ARE5, ARE6, ARE8 or ARE9. Luciferase activity was measured 24 h after transfection. Luciferase activities were normalized to renilla activity. Results are shown relative to control and are mean ± S.D. (n = 3). $^{**}p \leq 0.01$ according to a Student's t-test. See also Supplementary Table S1, Table S3, Table S4, Supplementary Fig. S4 and Fig. S5. (For interpretation of the references to colour in this figure legend, the reader is referred to the Web version of this article.)

neurospheres. Moreover, glioma stem cell frequency was decreased as determined in limiting dilution assays (Supplementary Table S5A), demonstrating that both proteins are required for cancer stem cell growth. In rescue experiments, we combined NRF2 knock-down with ectopic retroviral expression of TAZ in glioblastomas explants GB1 (Fig. 6G- **6I**), GB3, (Fig. S6J- 6L), U-87 MG (Supplementary Fig. 6A-C) and U-373 MG (Supplementary Fig. 6D- 6F). Regarding neurosphere growth (Fig. 6H, I, K, L, Supplementary Figs. S6B, S6C, S6E and S6F), TAZ also partially rescued the number of neurospheres and glioma stem cell frequency (Supplementary Table S5B). Altogether, these results point to TAZ as an instrumental effector of NRF2-driven cancer stem cell growth.

3.6. The NRF2/TAZ axis is essential for tumorigenesis of GBs

We assessed the tumorigenicity of NRF2- or TAZ-knocked down glioma stem cells in xenotransplanted athymic mice. The growth of subcutaneous xenografts was substantially reduced by silencing the expression of either transcription factor in U-87 MG cells (Fig. 7A and 7B) or U-373 MG cells (Supplementary Figs. S7A and S7B). In mice intracranially inoculated with U-87 MG cells, the survival rate was roughly 30 days and increased up to 40 and 60 days by selective silencing of NRF2 or TAZ, respectively (Fig. 7C).

In order to better reproduce the human pathology, we orthotopically implanted GB3 primary tumor cells and monitored tumor formation in the brain by magnetic resonance imaging (Fig. 7D and E). These cells developed tumors that, like in humans, exhibited heterogeneous and diffused borders with peritumoral and systemic brain edema (Supplemental Fig. 7C). Primary GB3 cells developed tumors before 10 days. However, when the same cells were knocked-down for expression of NRF2 or TAZ, they did not generate tumors at least after 30 days (Fig. 7D and E).

In additional rescue experiments we tested the relevance of TAZ as an effector of NRF2-mediated tumorigenicity. TAZ over-expression in control cells expressing basal levels of NRF2 did not lead to a statistically significant increase in tumor volume. However, TAZ over-expression restored by 20% the growth of tumors derived from NRF2-knocked-down U-87 MG (Fig. 7F and G) and U-373 MG cells (Supplementary Figs. S7D and S7E). In intracranial tumors, mouse life expectancy decreased from 45 days in the control NRF2-silenced cells to 35 days in the TAZ rescued cells (Fig. 7H). These results indicate that TAZ is one effector of NRF2-induced tumorigenicity in GBs.

4. Discussion

An effective therapy for GB would be possible if its molecular pathology was better known. In the TCGA database we found that somatic mutations in the NRF2 and Hippo pathways are rare (Fig. 1A) whereas EGFR and PTEN mutations are very frequent. However, NRF2 levels were high in these glioma stem cells compared to the non-tumorigenic neural stem cell line ReNcell, therefore demonstrating an abnormal up-regulation of NRF2 in GBs. These results suggest that NRF2 activation might be connected with subversion of signaling pathways that impinge on EGFR or PTEN. We have previously reported that chemical or genetic inhibition of PTEN in prostate and endometrial cancers leads to the activation of NRF2. This is due to the constitutive inhibition of glycogen synthase kinase-3 (GSK-3), thus relieving NRF2 from the GSK-3/beta-TrCP ubiquitin-proteasome pathway [27,32,38].

We also found that the transcript levels of *WWTR1* exhibit the same trend as NRF2 to be increased in GBs, suggesting that they might be mechanistically connected. Genetic (shRNA and NRF2 overexpression) and chemical (sulforaphane) manipulation of NRF2 indicated that the transcript and protein levels of TAZ and TAZ-dependent genes are, at least in part, governed by the levels of NRF2. We have also observed that TAZ knock-down decreases NRF2 protein (Fig. 2D, F, 6A and 6D) but not transcript levels (Fig. 2C and E). One possible explanation is

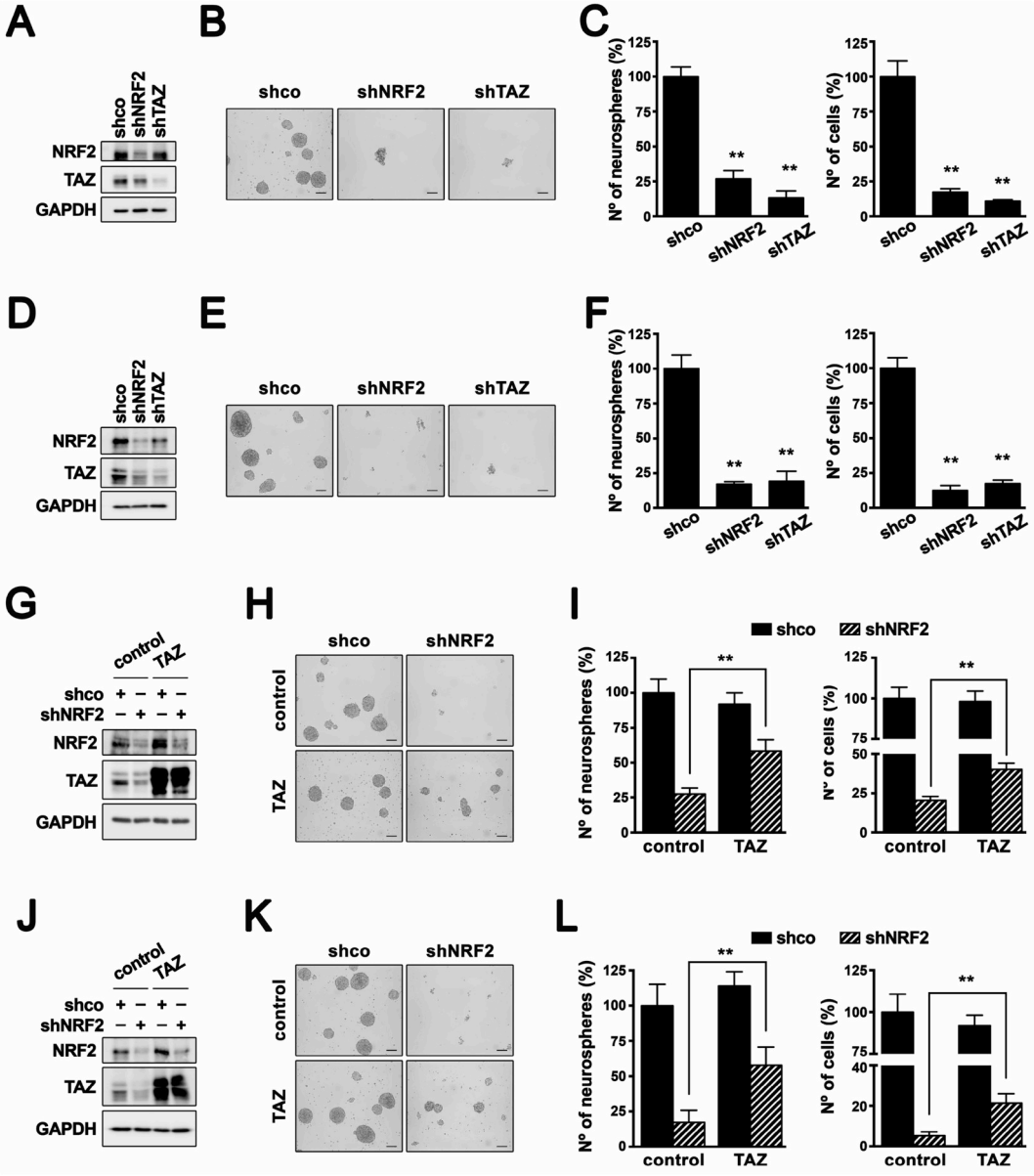

Fig. 6. Ectopic expression of TAZ rescues neurosphere growth of NRF2-knocked-down glioma stem cells GB1 **(A–C)** and GB3 **(D–F)** cells were transduced with lentivirus encoding shco, human shNRF2 or human shTAZ. **(A, D)** Representative immunoblot analysis of NRF2, TAZ and GAPDH as a loading control (n = 3). **(B, E)** Representative images of tumor neurosphere formation. Scale bar, 100 μm. **(C, F)** Quantification of the number of secondary neurospheres or the number of cells represented as percentage relative to shco. Data presented mean ± S.D. (n = 3) **p ≤ 0.01 according to a Student's t-test. GB1 **(G–I)** and GB3 **(J–L)** cells were transduced with empty retrovirus as control or a retrovirus expressing TAZ, and then with a lentivirus expressing shco or shNRF2. **(G, J)** Representative immunoblot analysis of NRF2, TAZ and GAPDH as a loading control (n = 3). **(H, K)** Representative images of tumor neurosphere formation. Scale bar, 100 μm. **(I, L)** Quantification of the number of secondary neurospheres and the number of cells represented as a percentage relative to control-shco. Data are presented as mean ± S.D. (n = 3) **p ≤ 0.01 according to a Student's t-test. See also Supplementary Fig. S6 and Supplementary Table S5.

that by silencing TAZ, there is a depletion in the expression of signaling genes such as CTGF and AREG of the EGF family of growth factors which by means of an autocrine loop might regulate NRF2 stability through GSK-3/beta-TRCP [17,27,32]. Because TAZ responds to stress signals, we analyzed if the changes in TAZ levels could be attributed to an indirect effect that might result from variations in oxidative stress when NRF2 is silenced. However, under cancer stem cell growth conditions, the depletion of NRF2 did not lead to measurable redox changes except in U-87 MG cells. Although at first glance this finding may seem surprising, it should be noted that up-regulation of NRF2 not only provides redox tolerance, but also a metabolic switch towards the pentose phosphate pathway that leads to NADPH and ribose production as precursors for cell growth and division. This metabolic reprograming may be particularly important in tumors with low growth rate where redox alterations are not so relevant and yet need growth precursors. In any case, the fact that U-87 MG submitted to GSH-MEE did not alter TAZ levels further suggests that NRF2 can regulate TAZ in a redox-independent manner.

We identified several putative AREs in the *WWTR1* gene promoter. The most potent ARE located at a highly DNAse-sensitive and H3K27-acetylated region, suggesting that it is accessible to the transcriptional machinery, but was not as potent as the canonical ARE of *HMOX1*, which is rapidly induced upon NRF2 activation. Several studies have analyzed the NRF2 transcriptional signature by microarray or RNA-sequencing approaches [8,39]. From these studies it is possible to distinguish grades of gene response to NRF2, from the most sensitive ones,

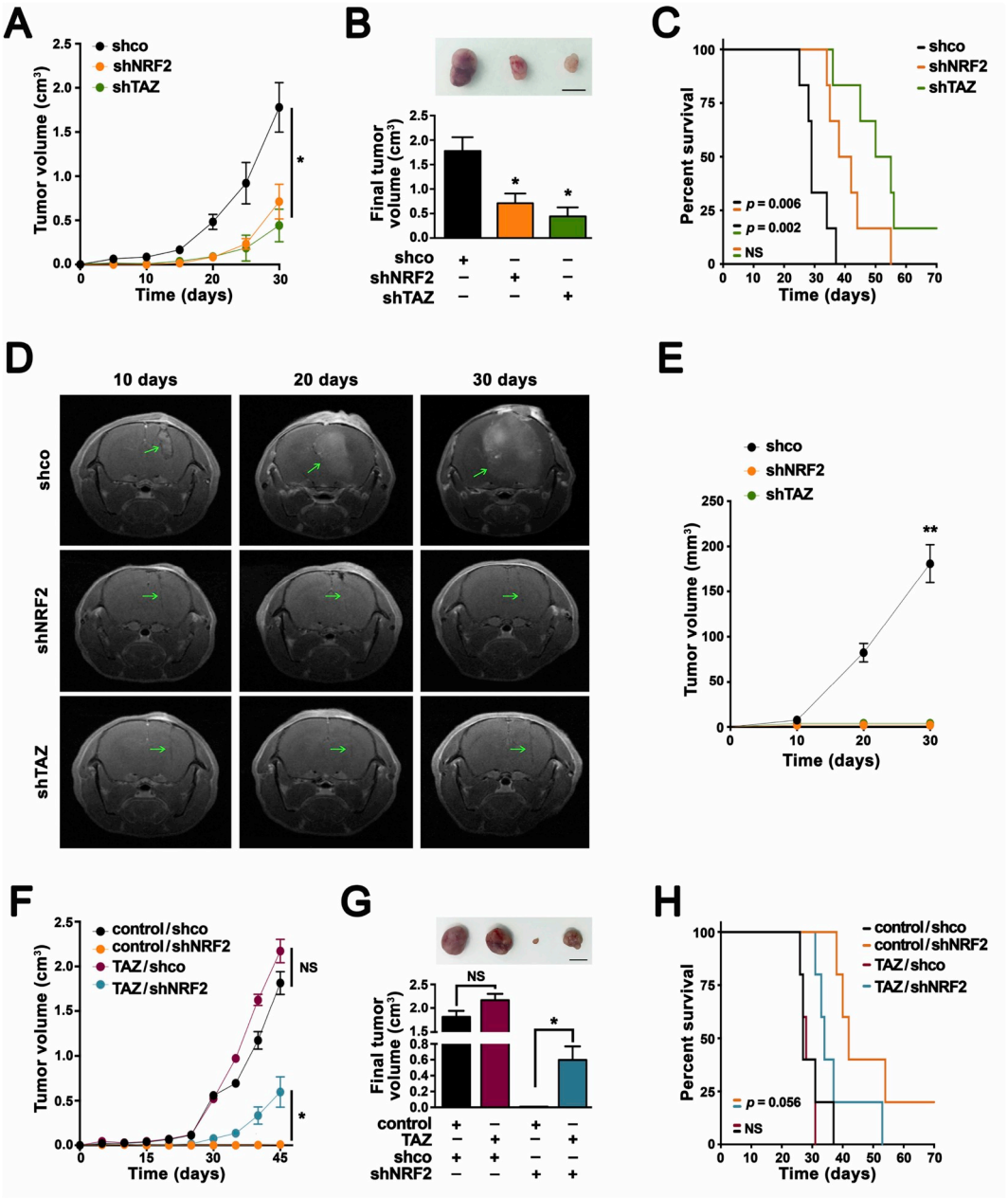

Fig. 7. The NRF2/TAZ axis is essential for tumorigenesis of GBs. **(A, B)** U-87 MG glioblastoma cells were transduced with a lentivirus encoding shco, human shNRF2 or human shTAZ and implanted subcutaneously in athymic mice. **(A)** Growth curves of xenograft tumors. Data are presented as mean ± S.E.M. (n = 4). *$p \leq 0.05$ according to a Student's t-test. **(B)** Upper panel, representative tumors of each experimental condition at the end point (scale bar, 1 cm); lower graph, quantification of the final tumor volume. Data are presented as mean ± S.E.M. (n = 4). *$p \leq 0.05$ according to a Student's t-test. **(C)** Kaplan-Meier survival curves of mice orthotopically implanted in the brain. Log-rank test between shco and shNRF2 is indicated (n = 6). **(D, E)** GB3 glioblastoma explant cells were transduced with a lentivirus encoding shco, human shNRF2 or human shTAZ and orthotopically implanted in the brain in athymic mice. **(D)** Representative image of T1 MRI of each experimental condition after 10, 20 and 30 days post-surgery. Green arrows indicate the tumor in shco or the injection scar in shNRF2 or shTAZ. **(E)** Growth curves of brain tumors. Data are presented as mean ± S.E.M. (n = 6) **$p \leq 0.01$ according to a Student's t-test. **(F, G)** U-87 MG cells were transduced with empty retrovirus or a retrovirus expressing TAZ and then with lentivirus encoding shco or shNRF2 and implanted subcutaneously in athymic mice. **(F)** Growth curves of xenograft tumors. Data are presented as mean ± S.E.M. (n = 4). *$p \leq 0.05$ according to a Student's t-test. **(G)** Upper panel, representative tumors of each experimental condition at the end point (scale bar, 1 cm); lower graph, quantification of the final tumor volume. Data are presented as mean ± S.E.M. (n = 4). *$p \leq 0.05$ according to a Student's t-test. **(H)** Kaplan-Meier survival curves of mice orthotopically implanted in the brain. Log-rank test between control/shNRF2 and TAZ/shNRF2: $p = 0.056$ (n = 5). See also Supplementary Fig. S7. (For interpretation of the references to colour in this figure legend, the reader is referred to the Web version of this article.)

related to the classical redox control, to others that need more time and persistent presence of NRF2. For instance, genes involved in metabolic reprograming or autophagy appear to require persistent exposure to NRF2 [26,40]. Therefore, we suggest that a low but persistent level of TAZ expression elicited by NRF2 may contribute to promotion of tumorigenesis in GBs. Considering that cell specific epigenetic changes may hinder regulatory sequences, the relevance of this NRF2/TAZ axis needs to be evaluated under the particular conditions of each cellular model.

Glioma stem cells were strictly dependent of NRF2 expression to develop spheroids and tumors, in agreement with a previous study [41], as NRF2 knocked-down xenografts exhibited a dramatic reduction

in tumor formation following subcutaneous and intracranial inoculation. Interestingly, TAZ overexpression partially restored stem cell growth and tumorigenicity, further demonstrating that TAZ is an effector of NRF2 to support stemness. However, this effect was modest, suggesting that NRF2 uses additional pathways to elicit tumorigenicity. In fact, besides it role in redox regulation, recent studies further suggest that NRF2 regulates pathways involved in tumorigenesis and self-renewal such as Shh ([42], Wnt [43] and Notch [44].

It would be expected that the Hippo pathway is silent in cancer cells for TAZ to remain transcriptionally active. However, among the 721 gliomas analyzed, only 4.4% exhibited mutations that might potentially inactivate the Hippo pathway (Fig. 1A and [45]). Moreover, TAZ expression was increased in these tumors, therefore indicating additional mechanisms for TAZ up-regulation. Our study identifies NRF2 as one such mechanism, hence probably counteracting repressor signals and providing a tumor growth advantage.

An efficient therapy for GBs must consider that high *NFE2L2* and *WWTR1* levels are predictors of chemoresistance [46,47]. Indeed, overexpression of NRF2 and TAZ correlated with resistance to the alkylating agent temozolomide, which is the gold standard treatment for gliomas. At this time, no selective NRF2 inhibitor is available, but at least as a proof-of-concept, we found that genetic knock-down of NRF2 drastically reduced TAZ transcriptional signature and stemness in gliomas. Contrary to *EGFR* and *PTEN*, the observation that *NFE2L2* is not frequently mutated in GBs and that yet NRF2 is strictly necessary to sustain tumorigenesis of glioblastoma stem cells provides a rationale to use drugs that could modulate NRF2 activity as a downstream effector of these mutated genes.

Authors contributions

ME, DL, MP, NRA, AIR and RFG conducted the experiments of molecular biology. MM, VMM and IE conducted tissue arrays. PLL conducted MRI data analysis. RG conducted massive data analysis. ME and AC designed the experiments and wrote the paper.

Declaration of competing interest

The authors declare no competing interests.

Acknowledgements

This study was funded by the Spanish Ministry of Economy and Competitiveness (MINECO) under the grant SAF2016-76520-R. ME is recipient of a postdoctoral contract Juan de la Cierva; DL and NRA of a FPU contract of MINECO; MP and RFG of a FPI contracts of Autonomous University of Madrid. RG has been funded by the AECC Scientific Foundation.

Appendix A. Supplementary data

Supplementary data to this article can be found online at https://doi.org/10.1016/j.redox.2019.101425.

References

[1] F. Hanif, K. Muzaffar, K. Perveen, S.M. Malhi, U. Simjee Sh, Glioblastoma multiforme: a review of its epidemiology and pathogenesis through clinical presentation and treatment, Asian Pac. J. Cancer Prev. APJCP 18 (2017) 3–9.

[2] A. Cuadrado, G. Manda, A. Hassan, M.J. Alcaraz, C. Barbas, A. Daiber, P. Ghezzi, R. Leon, M.G. Lopez, B. Oliva, M. Pajares, A.I. Rojo, N. Robledinos-Anton, A.M. Valverde, E. Guney, H. Schmidt, Transcription factor NRF2 as a therapeutic target for chronic diseases: a systems medicine approach, Pharmacol. Rev. 70 (2018) 348–383.

[3] J.D. Hayes, A.T. Dinkova-Kostova, The Nrf2 regulatory network provides an interface between redox and intermediary metabolism, Trends Biochem. Sci. 39 (2014) 199–218.

[4] S.B. Lee, B.N. Sellers, G.M. DeNicola, The regulation of NRF2 by nutrient-responsive signaling and its role in anabolic cancer metabolism, Antioxidants Redox Signal. 29 (2018) 1774–1791.

[5] G.M. DeNicola, F.A. Karreth, T.J. Humpton, A. Gopinathan, C. Wei, K. Frese, D. Mangal, K.H. Yu, C.J. Yeo, E.S. Calhoun, F. Scrimieri, J.M. Winter, R.H. Hruban, C. Iacobuzio-Donahue, S.E. Kern, I.A. Blair, D.A. Tuveson, Oncogene-induced Nrf2 transcription promotes ROS detoxification and tumorigenesis, Nature 475 (2011) 106–109.

[6] X.J. Wang, Z. Sun, N.F. Villeneuve, S. Zhang, F. Zhao, Y. Li, W. Chen, X. Yi, W. Zheng, G.T. Wondrak, P.K. Wong, D.D. Zhang, Nrf2 enhances resistance of cancer cells to chemotherapeutic drugs, the dark side of Nrf2, Carcinogenesis 29 (2008) 1235–1243.

[7] M.B. Sporn, K.T. Liby, NRF2 and cancer: the good, the bad and the importance of context, Nat. Rev. Cancer 12 (2012) 564–571.

[8] A. Namani, Q.Q. Cui, Y. Wu, H. Wang, X.J. Wang, X. Tang, NRF2-regulated metabolic gene signature as a prognostic biomarker in non-small cell lung cancer, Oncotarget 8 (2017) 69847–69862.

[9] B. Padmanabhan, K.I. Tong, T. Ohta, Y. Nakamura, M. Scharlock, M. Ohtsuji, M.I. Kang, A. Kobayashi, S. Yokoyama, M. Yamamoto, Structural basis for defects of Keap1 activity provoked by its point mutations in lung cancer, Mol. Cell 21 (2006) 689–700.

[10] Z.X. Cong, H.D. Wang, J.W. Wang, Y. Zhou, H. Pan, D.D. Zhang, L. Zhu, ERK and PI3K signaling cascades induce Nrf2 activation and regulate cell viability partly through Nrf2 in human glioblastoma cells, Oncol. Rep. 30 (2013) 715–722.

[11] M. Kanamori, T. Higa, Y. Sonoda, S. Murakami, M. Dodo, H. Kitamura, K. Taguchi, T. Shibata, M. Watanabe, H. Suzuki, I. Shibahara, R. Saito, Y. Yamashita, T. Kumabe, M. Yamamoto, H. Motohashi, T. Tominaga, Activation of the NRF2 pathway and its impact on the prognosis of anaplastic glioma patients, Neuro Oncol. 17 (2015) 555–565.

[12] T. Wu, B.G. Harder, P.K. Wong, J.E. Lang, D.D. Zhang, Oxidative stress, mammospheres and Nrf2-new implication for breast cancer therapy? Mol. Carcinog. 54 (2015) 1494–1502.

[13] J. Zhu, H. Wang, Y. Fan, Y. Hu, X. Ji, Q. Sun, H. Liu, Knockdown of nuclear factor erythroid 2-related factor 2 by lentivirus induces differentiation of glioma stem-like cells, Oncol. Rep. 32 (2014) 1170–1178.

[14] Y. Jia, J. Chen, H. Zhu, Z.H. Jia, M.H. Cui, Aberrantly elevated redox sensing factor Nrf2 promotes cancer stem cell survival via enhanced transcriptional regulation of ABCG2 and Bcl-2/Bmi-1 genes, Oncol. Rep. 34 (2015) 2296–2304.

[15] N. Wakabayashi, S. Shin, S.L. Slocum, E.S. Agoston, J. Wakabayashi, M.K. Kwak, V. Misra, S. Biswal, M. Yamamoto, T.W. Kensler, Regulation of notch1 signaling by nrf2: implications for tissue regeneration, Sci. Signal. 3 (2010) ra52.

[16] J. Zhu, H. Wang, Q. Sun, X. Ji, L. Zhu, Z. Cong, Y. Zhou, H. Liu, M. Zhou, Nrf2 is required to maintain the self-renewal of glioma stem cells, BMC Canc. 13 (2013) 380.

[17] T. Moroishi, C.G. Hansen, K.L. Guan, The emerging roles of YAP and TAZ in cancer, Nat. Rev. Cancer 15 (2015) 73–79.

[18] X. Zhou, Q.Y. Lei, Regulation of TAZ in cancer, Protein Cell 7 (2016) 548–561.

[19] K.P. Bhat, K.L. Salazar, V. Balasubramaniyan, K. Wani, L. Heathcock, F. Hollingsworth, J.D. James, J. Gumin, K.L. Diefes, S.H. Kim, A. Turski, Y. Azodi, Y. Yang, T. Doucette, H. Colman, E.P. Sulman, F.F. Lang, G. Rao, S. Copray, B.D. Vaillant, K.D. Aldape, The transcriptional coactivator TAZ regulates mesenchymal differentiation in malignant glioma, Genes Dev. 25 (2011) 2594–2609.

[20] X. Zhou, Z. Wang, W. Huang, Q.Y. Lei, G protein-coupled receptors: bridging the gap from the extracellular signals to the Hippo pathway, Acta Biochim. Biophys. Sin. 47 (2015) 10–15.

[21] S. Dupont, L. Morsut, M. Aragona, E. Enzo, S. Giulitti, M. Cordenonsi, F. Zanconato, J. Le Digabel, M. Forcato, S. Bicciato, N. Elvassore, S. Piccolo, Role of YAP/TAZ in mechanotransduction, Nature 474 (2011) 179–183.

[22] F.X. Yu, K.L. Guan, The Hippo pathway: regulators and regulations, Genes Dev. 27 (2013) 355–371.

[23] C.Y. Liu, Z.Y. Zha, X. Zhou, H. Zhang, W. Huang, D. Zhao, T. Li, S.W. Chan, C.J. Lim, W. Hong, S. Zhao, Y. Xiong, Q.Y. Lei, K.L. Guan, The hippo tumor pathway promotes TAZ degradation by phosphorylating a phosphodegron and recruiting the SCF{beta}-TrCP E3 ligase, J. Biol. Chem. 285 (2010) 37159–37169.

[24] R. Gargini, J.P. Cerliani, M. Escoll, I.M. Anton, F. Wandosell, Cancer stem cell-like phenotype and survival are coordinately regulated by Akt/FoxO/Bim pathway, Stem Cells (Dayton) 33 (2015) 646–660.

[25] Y. Hu, G.K. Smyth, ELDA: extreme limiting dilution analysis for comparing depleted and enriched populations in stem cell and other assays, J. Immunol. Methods 347 (2009) 70–78.

[26] M. Pajares, N. Jimenez-Moreno, A.J. Garcia-Yague, M. Escoll, M.L. de Ceballos, F. Van Leuven, A. Rabano, M. Yamamoto, A.I. Rojo, A. Cuadrado, Transcription factor NFE2L2/NRF2 is a regulator of macroautophagy genes, Autophagy 12 (2016) 1902–1916.

[27] P. Rada, A.I. Rojo, S. Chowdhry, M. McMahon, J.D. Hayes, A. Cuadrado, SCF/{beta}-TrCP promotes glycogen synthase kinase 3-dependent degradation of the Nrf2 transcription factor in a Keap1-independent manner, Mol. Cell. Biol. 31 (2011) 1121–1133.

[28] A.I. Rojo, N.G. Innamorato, A.M. Martin-Moreno, M.L. De Ceballos, M. Yamamoto, A. Cuadrado, Nrf2 regulates microglial dynamics and neuroinflammation in experimental Parkinson's disease, Glia 58 (2010) 588–598.

[29] M. Escoll, R. Gargini, A. Cuadrado, I.M. Anton, F. Wandosell, Mutant p53 oncogenic functions in cancer stem cells are regulated by WIP through YAP/TAZ, Oncogene 36 (2017) 3515–3527.

[30] R. Gargini, M. Escoll, E. Garcia, R. Garcia-Escudero, F. Wandosell, I.M. Anton, WIP drives tumor progression through YAP/TAZ-Dependent autonomous cell growth, Cell Rep. 17 (2016) 1962–1977.

[31] M. Pajares, A.I. Rojo, E. Arias, A. Diaz-Carretero, A.M. Cuervo, A. Cuadrado, Transcription factor NFE2L2/NRF2 modulates chaperone-mediated autophagy through the regulation of LAMP2A, Autophagy 14 (2018) 1310–1322.
[32] P. Rada, A.I. Rojo, N. Evrard-Todeschi, N.G. Innamorato, A. Cotte, T. Jaworski, J.C. Tobon-Velasco, H. Devijver, M.F. Garcia-Mayoral, F. Van Leuven, J.D. Hayes, G. Bertho, A. Cuadrado, Structural and functional characterization of Nrf2 degradation by the glycogen synthase kinase 3/beta-TrCP axis, Mol. Cell. Biol. 32 (2012) 3486–3499.
[33] H. Ohgaki, P. Kleihues, The definition of primary and secondary glioblastoma, Clin. Cancer Res. 19 (2013) 764–772.
[34] T.M. Malta, C.F. de Souza, T.S. Sabedot, T.C. Silva, M.S. Mosella, S.N. Kalkanis, J. Snyder, A.V.B. Castro, H. Noushmehr, Glioma CpG island methylator phenotype (G-CIMP): biological and clinical implications, Neuro Oncol. 20 (2018) 608–620.
[35] J. Zhu, H. Wang, X. Ji, L. Zhu, Q. Sun, Z. Cong, Y. Zhou, H. Liu, M. Zhou, Differential Nrf2 expression between glioma stem cells and non-stem-like cells in glioblastoma, Oncol. Lett. 7 (2014) 693–698.
[36] M. McMahon, K. Itoh, M. Yamamoto, J.D. Hayes, Keap1-dependent proteasomal degradation of transcription factor Nrf2 contributes to the negative regulation of antioxidant response element-driven gene expression, J. Biol. Chem. 278 (2003) 21592–21600.
[37] M.E. Hardee, A.E. Marciscano, C.M. Medina-Ramirez, D. Zagzag, A. Narayana, S.M. Lonning, M.H. Barcellos-Hoff, Resistance of glioblastoma-initiating cells to radiation mediated by the tumor microenvironment can be abolished by inhibiting transforming growth factor-beta, Cancer Res. 72 (2012) 4119–4129.
[38] A. Cuadrado, Structural and functional characterization of Nrf2 degradation by glycogen synthase kinase 3/beta-TrCP, Free Radic. Biol. Med. 88 (2015) 147–157.
[39] B.N. Chorley, M.R. Campbell, X. Wang, M. Karaca, D. Sambandan, F. Bangura, P. Xue, J. Pi, S.R. Kleeberger, D.A. Bell, Identification of novel NRF2-regulated genes by ChIP-Seq: influence on retinoid X receptor alpha, Nucleic Acids Res. 40 (2012) 7416–7429.
[40] Y. Mitsuishi, K. Taguchi, Y. Kawatani, T. Shibata, T. Nukiwa, H. Aburatani, M. Yamamoto, H. Motohashi, Nrf2 redirects glucose and glutamine into anabolic pathways in metabolic reprogramming, Cancer Cell 22 (2012) 66–79.
[41] X.J. Ji, S.H. Chen, L. Zhu, H. Pan, Y. Zhou, W. Li, W.C. You, C.C. Gao, J.H. Zhu, K. Jiang, H.D. Wang, Knockdown of NF-E2-related factor 2 inhibits the proliferation and growth of U251MG human glioma cells in a mouse xenograft model, Oncol. Rep. 30 (2013) 157–164.
[42] J. Jang, Y. Wang, M.A. Lalli, E. Guzman, S.E. Godshalk, H. Zhou, K.S. Kosik, Primary cilium-autophagy-nrf2 (PAN) Axis Activation commits human embryonic stem cells to a neuroectoderm fate, Cell 165 (2016) 410–420.
[43] P. Rada, A.I. Rojo, A. Offergeld, G.J. Feng, J.P. Velasco-Martin, J.M. Gonzalez-Sancho, A.M. Valverde, T. Dale, J. Regadera, A. Cuadrado, WNT-3A regulates an Axin1/NRF2 complex that regulates antioxidant metabolism in hepatocytes, Antioxidants Redox Signal. 22 (2015) 555–571.
[44] N. Wakabayashi, J.J. Skoko, D.V. Chartoumpekis, S. Kimura, S.L. Slocum, K. Noda, D.L. Palliyaguru, M. Fujimuro, P.A. Boley, Y. Tanaka, N. Shigemura, S. Biswal, M. Yamamoto, T.W. Kensler, Notch-Nrf2 axis: regulation of Nrf2 gene expression and cytoprotection by notch signaling, Mol. Cell. Biol. 34 (2014) 653–663.
[45] F. Sanchez-Vega, M. Mina, J. Armenia, W.K. Chatila, A. Luna, K.C. La, S. Dimitriadoy, D.L. Liu, H.S. Kantheti, S. Saghafinia, D. Chakravarty, F. Daian, Q. Gao, M.H. Bailey, W.W. Liang, S.M. Foltz, I. Shmulevich, L. Ding, Z. Heins, A. Ochoa, B. Gross, J. Gao, H. Zhang, R. Kundra, C. Kandoth, I. Bahceci, L. Dervishi, U. Dogrusoz, W. Zhou, H. Shen, P.W. Laird, G.P. Way, C.S. Greene, H. Liang, Y. Xiao, C. Wang, A. Iavarone, A.H. Berger, T.G. Bivona, A.J. Lazar, G.D. Hammer, T. Giordano, L.N. Kwong, G. McArthur, C. Huang, A.D. Tward, M.J. Frederick, F. McCormick, M. Meyerson, E.M. Van Allen, A.D. Cherniack, G. Ciriello, C. Sander, N. Schultz, Oncogenic signaling pathways in the cancer genome Atlas, Cell 173 (2018) 321–337 e310.
[46] C.R. Rocha, G.S. Kajitani, A. Quinet, R.S. Fortunato, C.F. Menck, NRF2 and glutathione are key resistance mediators to temozolomide in glioma and melanoma cells, Oncotarget 7 (2016) 48081–48092.
[47] T. Tian, A. Li, H. Lu, R. Luo, M. Zhang, Z. Li, TAZ promotes temozolomide resistance by upregulating MCL-1 in human glioma cells, Biochem. Biophys. Res. Commun. 463 (2015) 638–643.